RSC Advances




ROYAL SOCIETY OF CHEMISTRY

www.rsc.org/advances

# Size-dependent thermal decomposition and kinetics of ultrafine alkali metal styphnates

Rui Liu[a], Wenyuan Zhao[a], Tonglai Zhang[a,*], Li Yang[a], Zunning Zhou[a], Shuyuan Qi[a]

Three alkali metal styphnates, $K_2$TNR, $Rb_2$TNR and $Cs_2$TNR, were fabricated into different particle sizes by the crystal-morphology-control microemulsion synthesis. The thermal decomposition and kinetics were studied by DSC and DPTA techniques. As the particle size decreases, the thermodynamic and kinetic parameters decrease while the decomposition gas amounts and reaction rate constants increase. The reduction in particle size leads to an increase in reactivity and a decrease in thermal stability. The thermal sensitivity determined by 5s explosion temperature and flame sensitivity grows with decreasing particle size. The ultrafine materials have small particle size and large specific surface area, and therefore possesses strong surface bonding energy, low activation energy barrier and high reactivity. In the case of the same size, the increasing order of thermal stability is $Cs_2$TNR < $Rb_2$TNR < $K_2$TNR. The central metal of small atomic radius has strong coordination bonding energy and therefore determines the high stability.



[a] *School of Mechatronic Engineering, Beijing Institute of Technology. No.5, Zhongguancun South Street, Beijing, 100081(China). Tel & Fax: (+8610) 68911202. E-mail: ztlbit@bit.edu.cn (corresponding author: Tonglai Zhang)*

*b China North Industries Corporation. No.12, Guanganmen South Street, Beijing, 100081 (China). Tel：010-83918383. E-mail: qsy@norinco.cn*

# Introduction

The ultrafine materials in micron- and nano sizes show many excellent properties in chemistry [1,2], medicine [3,4], biology [5,6], mechanics [7,8] and electromagnetism [9,10] compared to the bulk counterparts, thanks to their very small size and large surface characteristics. The particle refinement has become one of the hottest topics of materials science, and especially opens up new applications for the ultrafine energetic materials in the field of high-performance and high-safety munitions and aerospace propulsion system [11-14]. There are many feasible methods for particle refinement, such as mechanical grinding method [15], sol-gel method [16,17], solvent-non-solvent recrystallization [18,19], chemical vapor deposition [20,21], microemulsion synthesis [22-24] and crystal-morphology-control synthesis [25-27]. However, there is still great challenge to prepare the ultrafine energetic materials by a safe and convenient method.

Styphnic acid, whose chemically formal name is 2,4,6-trinitroresorcinol (see **Scheme 1**), is a very hazardous energetic material for its easy detonation at rapid heating [28,29]. It is also an important raw material for preparing the metal styphnates which are used as initiating explosives in the missile and space launch applications [30,31]. Lead styphnate is the best known explosive that has low initiating capability but high flame sensitivity. It has been used as a component of ignition charge in detonator [32]. Current research of metal styphnates is focused on the improvement in explosive performance and safety [33-35]. Unfortunately, as very important factors for safety evaluation, the morphology optimization and particle refinement of metal styphnates has received little attention, and the particle size dependence on the thermal properties is still inadequately known.

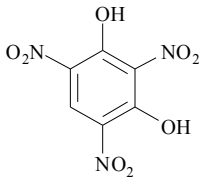


**Scheme 1** Chemical structure of styphnic acid——2,4,6-trinitroresorcinol.

In this work, three alkali metal styphnates, which are potassium, rubidium and cesium styphnates ($K_2$TNR, $Rb_2$TNR and $Cs_2$TNR), were prepared into three micron sizes respectively using the combination method of microemulsion and crystal-morphology-control for the first time.

It is an effective and safe method especially suitable for energetic materials, because the synthesis, refinement and morphology-control processes are completed synchronously. The thermal decomposition and kinetics of the styphnates were investigated by differential scanning calorimetry (DSC) and dynamic pressure measuring thermal analysis (DPTA). It is based on the principles that DSC deals with an open system where the reaction goes to completion, whilst DTPA deals with a closed tube where the partial pressure of evolved gases plays an important role in achieving the equilibrium. Moreover, the thermal explosion performances were assessed by the sensitivity tests. The size-dependent thermal behaviors, kinetics and thermodynamics, and thermal stability were studied.

# Experimental

### Preparation and refinement

$K_2TNR$, $Rb_2TNR$ and $Cs_2TNR$ were prepared by the improved method (**Scheme 2**) [36-38].

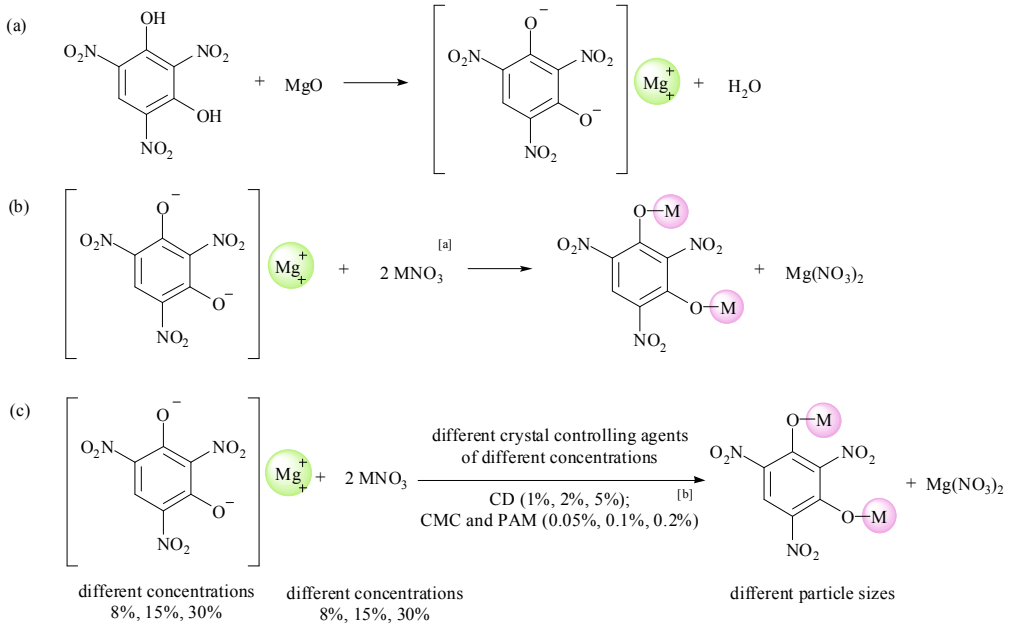


[a] M represents alkali metal, M = K, Rb, Cs

[b] The concentrations were determined according to their critical micelle concentrations.

**Scheme 2** Preparation processes of $M_2TNR$: (a) preparation of MgTNR; (b) preparation of coarse $M_2TNR$; (c) preparation of ultrafine $M_2TNR$ under the action of crystal-control reagents.

The information of the materials used in this work is summarized in **Table 1**.

**Table 1** Information of the materials used in this work.

| Name | Formula | State | Purity | Source |
|---|---|---|---|---|
| styphnic acid (2,4,6-trinitroresorcinol) | $H_2TNR$ | solid | > 98.0 % [c] | Meryer Chemical Technology Co., Ltd. |
| Magnesium oxide | MgO | solid | ≥ 98.5 % | Sinopharm Chemical Reagent Co.,Ltd. |
| Potassium nitrate | $KNO_3$ | solid | ≥ 99.0 % | Sinopharm Chemical Reagent Co.,Ltd. |
| Rubidium nitrate | $RbNO_3$ | solid | ≥ 99.5 % | Sinopharm Chemical Reagent Co.,Ltd. |
| Cesium nitrate | $CsNO_3$ | solid | ≥ 99.5 % | Sinopharm Chemical Reagent Co.,Ltd. |
| *β*-cyclodextrin | CD | solid | ≥ 98.0 % | Sigma-Aldrich Co.,Ltd. |
| Sodium carboxyl methyl cellulose [a] | CMC | solid | ≥ 99.5 % | Sigma-Aldrich Co.,Ltd. |
| Polyacrylamide [b] | PAM | solid | ≥ 98.0 % | Sigma-Aldrich Co.,Ltd. |

[a] The average molecular weight $M_w$=250000.

[b] The average molecular weight $M_w$=400000.

[c] Weight percentage.

*Caution!* The energetic materials posing flammable and explosive hazard should be treated in small batches with proper precautions. 5.00 g (0.02 mol) $H_2TNR$ and 0.81 g (0.02 mol) MgO were mixed and added into 300 ml distilled water. The mixture solution was stirred at 60 $^oC$ until a dark brown solution was formed. The MgTNR solution was obtained by instant filtration. Then, 4.05 g (0.04 mol) $KNO_3$ and 5.90 g (0.04 mol) $RbNO_3$ and 7.80 g (0.04 mol) $CsNO_3$ were dissolved in 50 ml distilled water, respectively. Each solution was added slowly into MgTNR solution under constant stirring at 60 $^oC$. When the mixture solution turned turbid, it was rapidly transferred into a low-temperature chemical reaction apparatus. After the yellow crystals were precipitated, the product $M_2TNR$ was obtained through filtration and washing by distilled water and anhydrous ethyl alcohol (in order to wash away crystal-control reagent and any other impurities that might be weakly physisorbed) and then placed in a water-bath drying oven at 55 $^oC$. The yields ranged from 75 to 85 %.

The ultrafine $M_2TNR$ were prepared by adding crystal-control reagent of different kinds and concentrations in a given synthesis step while keeping other conditions the same (**Scheme 2c**). CD, CMC and PAM were selected empirically as available crystal-control reagents. All the resulting $M_2TNR$s were purified through recrystalization up to more than 99 %. To avoid the influence of the impurity adsorbed gases, the prepared samples were vacuum-dried in 40 ºC for 12 h and then stored in a desiccator below room temperature until use.

### Apparatus and methods

BX51-P polarizing microscope (Olympus, Japan) was used to observe the morphology of sample under illumination mode of transmitted light. Sample was dispersed in anhydrous ethanol and placed on a slide.

FBRM-V6.7.0 online particle size analyzer (Mettler Toledo, Switzerland) was applied under dynamic air atmosphere with the pressure of 0.4 MPa. Sample was dispersed in hexane dispersant.

Pyris-1 DSC (Perkin-Elmer, USA) was used to study the complete thermal decomposition at high temperature. Less than 0.5 mg of sample was distributed evenly in an uncovered aluminum crucible and heated from 50 to 500 ºC at 5, 10, 15 and 20 ºC $min^{-1}$ respectively in dynamic nitrogen atmosphere of 20 ml $min^{-1}$.

DPTA, formerly known as dynamic vacuum stability test (DVST), was established based on the principle of vacuum stability test (VST) [39,40]. It is used to research the initial stage of thermal decomposition in low temperature range of 25~200 ºC. The built-in mini-sensors measure the absolute pressure of evolved gas and temperature consecutively and directly. The explosion-proof glass test tube has good heat conduction which maintains consistent temperatures between thermostat and reactant, and it also avoids heterogeneous catalysis caused by metallic tube wall. (1.0000±0.0010) g sample was loaded evenly in the bottom of the test tube. After being sealed and evacuated bellow 0.10 kPa, the tube was put into thermostat, and heated from room temperature to target temperature at heating rate ≤ 3 ºC $min^{-1}$, and then kept warm at this temperature for 48 h. The target temperatures were set from 60 to 140 ºC with increments of 20 ºC.

## Results and discussion

### Particle size and distribution

Three alkali metal styphnates were prepared into various micron sizes by regulating the kind and concentration of crystal-control reagent used. The results found that all the $M_2$TNRs were adjusted into ideal morphology and size only under the action of CD. The as-prepared $M_2$TNRs possess substantially similar appearance under the same amount of crystal-control reagent, though the ligand TNR coordinates with different central metals. Take $K_2$TNR as an example, and more

detailed morphology and particle size distribution are shown in **Figs. 1~2**.

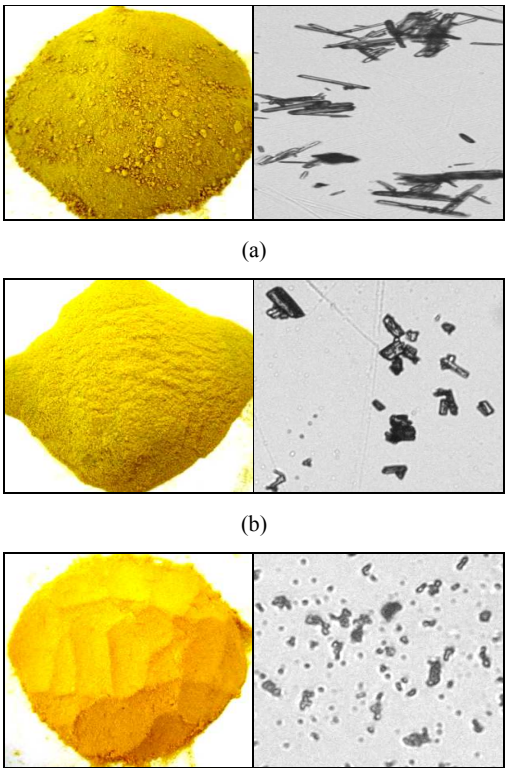

(a)

(b)

(c)

**Fig. 1** Morphologies of $K_2TNRs$: (a) $K_2TNR$-0; (b) $K_2TNR$-1; (c) $K_2TNR$-2.

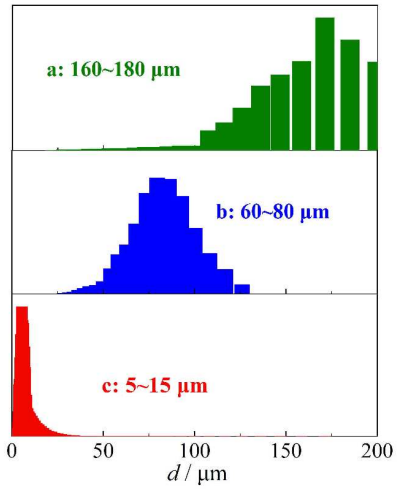


**Fig. 2** Particle size distribution of $K_2TNRs$: (a) $K_2TNR$-0; (b) $K_2TNR$-1; (c) $K_2TNR$-2.

The coarse $K_2TNR$ labeled $K_2TNR$-0 was synthesized without the presence of crystal-control reagent. It possesses a slender and needlelike shape with a length of 160~180 μm. The refined product $K_2TNR$-1 was obtained by adding 2 wt% CD to 8 wt% MgTNR and 8 wt% $KNO_3$,

respectively. It has an appearance of prism with a length of 60~80 μm and a width of 30~40μm. The smaller $K_2$TNR-2 was refined by the reaction of 15 wt% MgTNR and 15 wt% $KNO_3$ both of which were added 2 wt% CD, showing a likeness of ellipsoid with a long diameter of 5~15 μm. As the relative concentration of CD in the mixture solution reduced, the particle size of $M_2$TNR was refined from hundred to several micron, the morphology was gradually approaching to sphere, and the fluidity and dispersion became more regular and more uniform. According to Curie-Wulff principle [41], the vertical growth rate of the crystal face is proportional to its surface tension. The crystal-control reagent covers some specified crystal faces by electrostatic attraction, coordination bonding, hydrogen bonding, or van der Waals interaction. It not only reduces the surface tension of the formed crystal but also increases the diffusion coefficient of solute and the viscosity of solution, which lead to a decrease in the rates of nucleation and crystal-growth [42-46]. Thus, the $M_2$TNR crystal tends to grow into micron-sized spheroid and form into different sizes by varying the concentration of reagent. Furthermore, the same crystal-control reagent has the same effect on the improvement of the morphology and size of the styphnates which are coordinated with different metals. It suggests that the control mechanism of the crystal-control reagent is probably the same for different styphnates, though the detail is still ambiguous. Deep insight in this point will be studied in the future.

**DSC analysis**

The DSC curves of different-sized $M_2$TNRs under several heating rates were recorded. Only a single sharp exothermic decomposition process has been observed for all $M_2$TNRs, and the curves at 10 $^{o}$C min$^{-1}$ are taken as examples in **Fig. 3**.

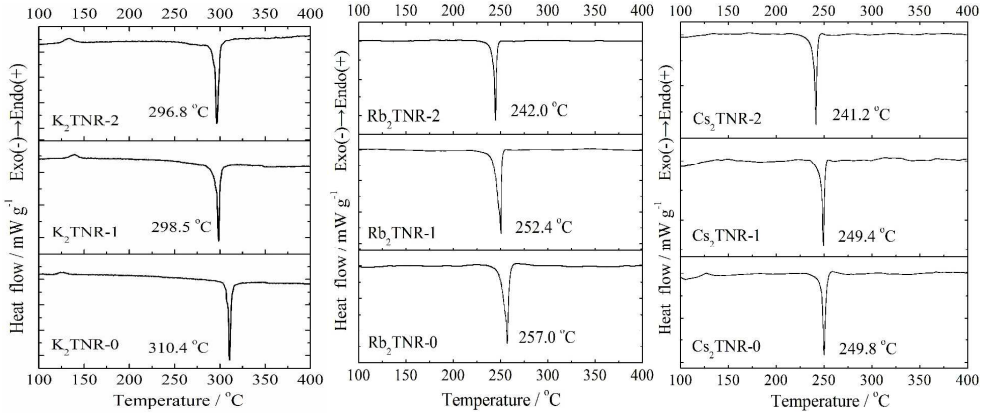

(a) (b) (c)

**Fig. 3** DSC curves of $K_2$TNR (a), $Rb_2$TNR (b) and $Cs_2$TNR (c) with different particle sizes at 10 °C $min^{-1}$.

The critical temperature of thermal explosion ($T_b$) and the self accelerating decomposition temperature ($T_{SADT}$) are generally indicators of thermal safety for energetic materials [47]. The temperatures can be determined by Zhang-hu-xie-li method (Eq. 1)[48-50] and Semenov method (Eq.2)[51] respectively based on the peak temperature ($T_p$) shifting with heating rate ($\beta$).

$$T_p = T_{p0} + a_1\beta_i + a_2\beta_i^2 + \ldots + a_{L-2}\beta_i^{L-2} \quad (1)$$

$$T_b = \frac{E_{ao} - \left(E_{ao}^2 - 4E_{ao}RT_{p0}\right)^{1/2}}{2R} \quad (2)$$

where i=1, 2, …., $L$; $L$ represents the times of the tests at different heating rates; $a_1$, $a_2$, $a_3$, …, and $a_{L-2}$ are coefficient. Here $L = 4$, $T_p = T_{p0} + a_1\beta_i + a_2\beta_i^2$.

The characteristic temperatures of DSC are presented in **Table 2**.

**Table 2** Characteristic temperatures of $M_2$TNRs from DSC data [a].

| Sample | $\beta$ / °C $min^{-1}$ | $K_2$TNR | | | $Rb_2$TNR | | | $Cs_2$TNR | | |
|---|---|---|---|---|---|---|---|---|---|---|
| | | $T_p$ / °C | $T_b$ / °C | $T_{SADT}$ / °C | $T_p$ / °C | $T_b$ / °C | $T_{SADT}$ / °C | $T_p$ / °C | $T_b$ / °C | $T_{SADT}$ / °C |
| $M_2$TNR-0 | 5 | 302.6 | 306.17 | 293.95 | 249.8 | 255.18 | 245.15 | 240.9 | 247.46 | 234.50 |
| | 10 | 310.4 | | | 257.0 | | | 249.8 | | |
| | 15 | 314.8 | | | 257.3 | | | 251.3 | | |
| | 20 | 319.2 | | | 263.3 | | | 258.6 | | |
| $M_2$TNR-1 | 5 | 288.6 | 291.33 | 277.75 | 249.2 | 259.43 | 249.13 | 240.5 | 246.79 | 233.80 |
| | 10 | 298.5 | | | 252.4 | | | 249.4 | | |
| | 15 | 302.5 | | | 254.9 | | | 251.2 | | |
| | 20 | 307.2 | | | 261.8 | | | 258.3 | | |
| $M_2$TNR-2 | 5 | 284.3 | 284.59 | 269.95 | 240.1 | 251.48 | 234.88 | 239.3 | 252.59 | 237.25 |
| | 10 | 296.8 | | | 242.0 | | | 241.2 | | |
| | 15 | 300.1 | | | 253.7 | | | 250.0 | | |
| | 20 | 304.0 | | | 257.7 | | | 256.3 | | |

[a] $\beta$—— heating rate; $T_p$—— peak temperature of exothermic decomposition; $T_b$—— critical temperature of thermal explosion; $T_{SADT}$—— self accelerating decomposition temperature.

According to **Table 2**, the $T_p$ increases with increasing heating rate and decreases with decreasing particle size at the same $\beta$. However, the $T_b$ and $T_{SADT}$ conform to different changing trends. Herein the particle size of $M_2$TNR affects the thermal safety in different degrees, but the

effects are not in linear proportion. Thus, the thermodynamic and kinetic parameters should be calculated for further evaluation of the thermal safety, and the results are listed in **Table 3**.

**Table 3** Thermodynamic and kinetic parameters of $M_2TNRs$ [a].

| Sample | Thermodynamic parameters | | | Kinetic parameters | | | | |
|---|---|---|---|---|---|---|---|---|
| | $\Delta H^{\neq}$ / kJ mol$^{-1}$ | $\Delta S^{\neq}$ / J K$^{-1}$ mol$^{-1}$ | $\Delta G^{\neq}$ / kJ mol$^{-1}$ | $E_{aK}$ / kJ mol$^{-1}$ | lg ($A_K$/s$^{-1}$) | $-r_K$ | $E_{aO}$ / kJ mol$^{-1}$ | $-r_O$ |
| $K_2TNR$-0 | 225.81 | 100.57 | 168.77 | 230.52 | 18.76 | 0.9983 | 238.44 | 0.9984 |
| $K_2TNR$-1 | 191.06 | 47.59 | 164.84 | 195.64 | 15.98 | 0.9971 | 195.06 | 0.9973 |
| $K_2TNR$-2 | 171.90 | 14.97 | 163.77 | 176.41 | 14.27 | 0.9860 | 176.72 | 0.9873 |
| $Rb_2TNR$-0 | 230.13 | 151.47 | 151.63 | 234.44 | 21.38 | 0.9558 | 231.31 | 0.9588 |
| $Rb_2TNR$-1 | 227.57 | 148.34 | 150.09 | 231.91 | 21.22 | 0.9159 | 228.90 | 0.9213 |
| $Rb_2TNR$-2 | 132.06 | -33.67 | 149.16 | 136.28 | 11.70 | 0.9123 | 137.84 | 0.9214 |
| $Cs_2TNR$-0 | 169.92 | 39.84 | 149.69 | 174.14 | 15.54 | 0.9705 | 173.86 | 0.9732 |
| $Cs_2TNR$-1 | 169.01 | 38.13 | 149.67 | 173.22 | 15.45 | 0.9748 | 172.98 | 0.9771 |
| $Cs_2TNR$-2 | 144.68 | -7.87 | 148.70 | 148.93 | 13.06 | 0.9123 | 149.85 | 0.9207 |

[a] $\Delta S^{\neq}$—— entropy of activation; $\Delta H^{\neq}$—— enthalpy of activation; $\Delta G^{\neq}$—— free energy of activation; $E_a$—— apparent activation energy; $A$—— pre-exponential factor, the subscript K and O indicate the parameters were calculated by the Kissinger and Ozawa methods [51], respectively.

Obviously, the thermodynamic and kinetic parameters are both in direct proportion to particle size, ranking in order of $M_2TNR$-2 < $M_2TNR$-1 < $M_2TNR$-0. Theoretically, $\Delta H^{\neq} > 0$ indicates that the forward activation reaction is endothermic, and the smaller $\Delta H^{\neq}$ means the lower heat required to start the reaction, making it less endothermic. The decomposition therefore becomes more thermodynamically favorable as the particle size get smaller. $\Delta S^{\neq}$ signifies the difference of freedom degrees between activated transition state and reactant. The smallest-sized $M_2TNR$-2 has the most negative value of $\Delta S^{\neq}$, which implies that the transition state is most probably the chemically bonded compound of two or more species rather than several dissociated monomers. $\Delta G^{\neq} > 0$ indicates the thermal decomposition is not spontaneous. The $\Delta G^{\neq}$ decreases with decreasing particle size, which demonstrates the thermal decomposition of the smaller-sized material has lower barrier height and faster rate according to transition state theory $k = (RT/Nh)\exp(-\Delta G^{\neq}/RT)$. Thus, the decomposition of the smallest-sized $M_2TNR$-2 is more kinetically favorable than the others. It can be concluded that the thermal decomposition initiation of $M_2TNR$ become more preferential both in thermodynamics and kinetics as its particle size gets smaller. In terms of kinetics, $E_a$ signifies the minimum energy level that the colliding molecules

must possess in order to undergo a given chemical reaction [52]. The smaller-sized material has lower activation energy and lower decomposition temperature, and therefore can be initiated easily. The ultrafine material has very small size and large surface area which produce an increase of the active sites on the interface, a rise of the surface bonding energy, as well as an increase of the efficient collision probability among the reactant molecules [53-56]. Therefore, the particle refinement promotes the decomposition reactivity. Moreover, the linear relationship is obviously seen between the calculated Arrhenius parameters, $E_a$ and lg $A$. It can be concluded that the kinetic compensation effect exists among the thermal decomposition of each group of $M_2$TNR [57,58]. It indicates that the decompositions of $M_2$TNRs with different sizes (with the same central metals) include the same dominant and rate-determining reaction step, even though there are actually multiple steps occurring during the whole thermal decompositions [59-61]. Therefore, the single-step kinetic method can be applied adequately to represent the multi-step process with a single rate-determining step, obtaining the **apparent** kinetic parameters.

**DPTA analysis**

DPTA records the apparent evolved gas pressure ($p_{ap}$) changing with time. Errors due to thermal expansion and sensor drift/lag were corrected by standardization to obtain the net pressure at the conditions of 1.0 g sample mass, 25 mL volume and 273.15 K temperature. The time dependences of the net decomposition gas pressure ($p$-$t$) of $M_2$TNRs at 100 °C are shown in **Fig. 4**.

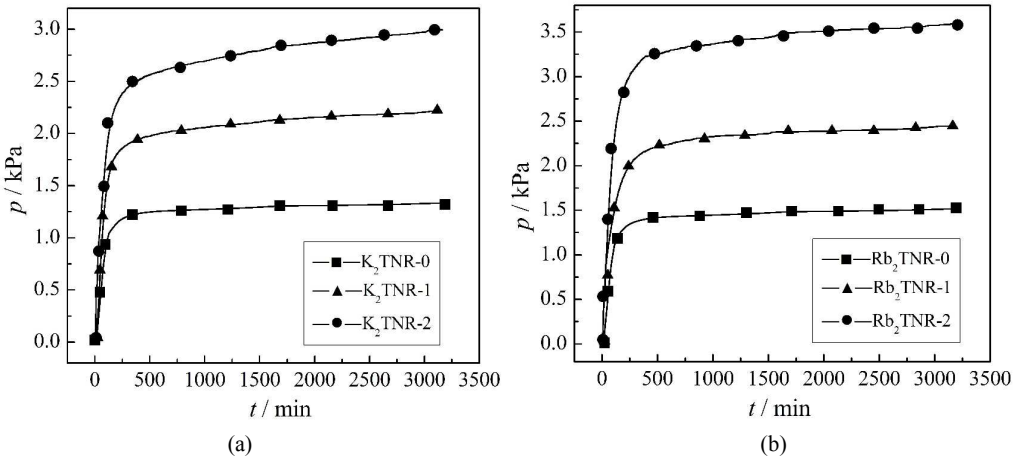

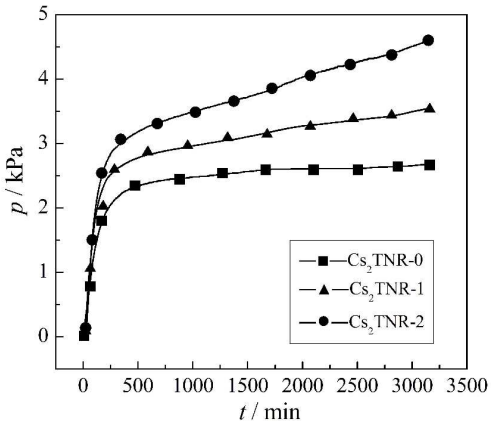


(c)

**Fig. 4** DPTA curves of $K_2$TNR (a), $Rb_2$TNR (b) and $Cs_2$TNR (c) with different sizes at 100 °C.

All the decomposition curves basically obey a parabolic trend with heating time. The curves consist of two stages: a rapid pressure rise while heating to the target temperature and a slow pressure growth at constant temperature. At the initial non-isothermal stage, the pressures increase rapidly with increasing temperature, but the largest pressure growth rate belongs to the smallest $M_2$TNR-2. At the following isothermal stage, the pressure growth rates slow gradually. The decompositions proceed slowly and smoothly in a long duration. On the whole, the total gas emission increases with decreasing particle size.

The DPTA tests were further carried out at various temperatures. The pressure is converted to the volume at the standard state (1.0 g sample, 101.325 kPa, and 273.15 K) as shown in **Table 4**.

**Table 4** Isothermal decomposition gas volumes of $M_2$TNRs at different temperatures.

| Sample | $V_i$ / mL $g^{-1}$ | | | | |
|---|---|---|---|---|---|
| | 60 °C | 80 °C | 100 °C | 120 °C | 140 °C |
| $K_2$TNR-0 | 0.035±0.003 | 0.119±0.008 | 0.252±0.016 | 0.320±0.019 | 0.528±0.031 |
| $K_2$TNR-1 | 0.092±0.007 | 0.182±0.012 | 0.420±0.027 | 0.562±0.034 | 0.783±0.045 |
| $K_2$TNR-2 | 0.173±0.012 | 0.320±0.022 | 0.568±0.037 | 0.824±0.049 | 1.108±0.064 |
| $Rb_2$TNR-0 | 0.099±0.007 | 0.147±0.010 | 0.286±0.019 | 0.448±0.037 | 0.694±0.040 |
| $Rb_2$TNR-1 | 0.156±0.011 | 0.231±0.016 | 0.462±0.030 | 0.688±0.041 | 0.972±0.056 |
| $Rb_2$TNR-2 | 0.218±0.015 | 0.356±0.024 | 0.682±0.044 | 0.944±0.057 | 1.294±0.075 |
| $Cs_2$TNR-0 | 0.166±0.012 | 0.261±0.018 | 0.506±0.033 | 0.852±0.051 | 1.268±0.074 |
| $Cs_2$TNR-1 | 0.225±0.016 | 0.388±0.026 | 0.668±0.043 | 1.011±0.061 | 1.490±0.086 |
| $Cs_2$TNR-2 | 0.332±0.023 | 0.545±0.037 | 0.874±0.057 | 1.204±0.072 | 1.808±0.104 |

For the same metal styphnate, the thermal stability increases as the particle size reduces

($M_2$TNR-2 < $M_2$TNR-1 < $M_2$TNR-0). The ultrafine particle has larger specific surface area and more activated atoms. These atoms have many dangling bonds or unsaturated bonds, making them easily react with the nearby atoms to form the stable state [13,62,63]. Thus, the minimization of the particle size decreases the thermal stability but increases the chemical reactivity. Through the Comparison of the different styphnates of the same particle size, the thermal stability increases in order of $Cs_2$TNR < $Rb_2$TNR < $K_2$TNR. The central metal plays a decisive role in evaluating the stability. The styphnate coordinated with the alkali metal of the small atomic number (small atomic radius) has strong bonding energy and therefore has high stability.

The amount of gas released at isothermal stage ($V_i$) is used to quantitatively characterize the thermal stability of energetic materials; less gas signifies greater stability. According to national military standard, good thermal stability requires the value of $V_i$ be < 2.00 mL $g^{-1}$ at 100 ºC [64,65]. As shown in **Table 4**, all samples have excellent thermal stability within the given temperature range though the gas volume increases with rising temperature.

The reaction rate constants at different temperatures were fitted by the solid phase reaction kinetic equation and listed in **Table 5**.

**Table 5** Reaction rate constants of $M_2$TNRs from DPTA data.

| Sample | $(10^6k)$ / $s^{-1}$ | | | | |
|---|---|---|---|---|---|
| | 60 °C | 80 °C | 100 °C | 120 °C | 140 °C |
| $K_2$TNR-0 | 2.51±0.21 | 4.26±0.35 | 5.62±0.45 | 6.88±0.55 | 9.25±0.74 |
| $K_2$TNR-1 | 2.74±0.23 | 4.80±0.39 | 5.85±0.47 | 7.34±0.59 | 9.36±0.75 |
| $K_2$TNR-2 | 2.89±0.25 | 4.88±0.40 | 6.23±0.50 | 7.77±0.62 | 9.65±0.77 |
| $Rb_2$TNR-0 | 1.81±0.15 | 3.78±0.31 | 5.53±0.44 | 6.23±0.50 | 8.90±0.71 |
| $Rb_2$TNR-1 | 2.13±0.18 | 4.67±0.38 | 5.81±0.46 | 6.75±0.54 | 9.23±0.74 |
| $Rb_2$TNR-2 | 2.54±0.22 | 4.79±0.39 | 6.05±0.48 | 7.20±0.58 | 9.31±0.75 |
| $Cs_2$TNR-0 | 1.67±0.14 | 3.76±0.31 | 5.41±0.43 | 5.68±0.46 | 8.86±0.71 |
| $Cs_2$TNR-1 | 1.86±0.16 | 4.52±0.37 | 5.57±0.45 | 5.94±0.48 | 8.93±0.72 |
| $Cs_2$TNR-2 | 2.02±0.17 | 4.63±0.38 | 5.89±0.47 | 6.42±0.51 | 8.96±0.72 |

For each $M_2$TNR, the reaction rate constant $k$ increase with increasing temperature, while at the same temperature it also increases with decreasing particle size ($M_2$TNR-0 < $M_2$TNR-1 < $M_2$TNR-2). On the one hand, the accelerating effect of high temperature on the reaction rate is beyond doubt. On the other hand, the refined material has larger specific surface area, endowing

the reaction interface with higher heat and mass transfer efficiency. Therefore, the thermal decomposition can also be accelerated by particle refinement.

**Thermal sensitivity**

The thermal sensitivity is evaluated by 5s explosion temperature ($T_{5s}$) [66] and flame sensitivity [67]. The resulting parameters are summarized in **Table 6**.

**Table 6** Thermal sensitivity parameters of $M_2$TNRs.

| Sample | 5s explosion temperature / °C | Flame sensitivity $H_{50\%}$ / cm[a] |
|---|---|---|
| $K_2$TNR-0 | 371.8 | 9 |
| $K_2$TNR-1 | 348.6 | 10 |
| $K_2$TNR-2 | 340.4 | 12 |
| $Rb_2$TNR-0 | 294.1 | 36 |
| $Rb_2$TNR-1 | 288.9 | 38 |
| $Rb_2$TNR-2 | 283.0 | 39 |
| $Cs_2$TNR-0 | 283.0 | 35 |
| $Cs_2$TNR-1 | 278.7 | 38 |
| $Cs_2$TNR-2 | 274.9 | 40 |

[a] Flame sensitivity is represented by the height corresponding to 50 % fire probability ($H_{50}$).

Theoretically, the lower $T_{5s}$ and higher $H_{50}$ denote the higher thermal sensitivity. Thus, the increasing sequence of thermal sensitivity is $M_2$TNR-0 < $M_2$TNR-1 < $M_2$TNR-2 which is identical to that of thermal decomposition activity. It suggests that the initiating mechanism of thermal explosion is probably the same as that of thermal decomposition [68-70]. The particle refinement also improves the thermal sensitivity. In fact, for energetic materials, the high stability does not necessarily mean superior functionality in some cases, because it also means low sensitivity. The suitable sensitivity is an important indicator of energy output level for energetic materials. Therefore, empirical determination of the optimum particle size is very necessary for balancing the stability and sensitivity and making the material achieve the best performance.

## Conclusions

Three alkali metal styphnates $M_2$TNRs were prepared and refined into different particle sizes. The thermal decomposition and kinetics were studied by DSC and DPTA techniques, and the thermal explosion performance was assessed by the sensitivity tests. The size-dependent thermal

properties of $M_2$TNRs were achieved. The following conclusions could be made:

(1) Under the action of crystal-control reagent, $M_2$TNR is effectively refined into three micron sizes. The morphology, fluidity and dispersion are also improved. The material of optimal morphology is prepared as small as 5~15 μm by the reaction of (15 wt% MgTNR+2 wt% CD) and (15 wt% $KNO_3$+2 wt% CD).

(2) According to DSC analysis, the thermodynamic and kinetic parameters are ranked in the same increasing order of $M_2$TNR-2 < $M_2$TNR-1 < $M_2$TNR-0. The reduction in particle size produces an increase in reactivity. The decomposition gas amounts and reaction rate constants obtained by DPTA analysis indicate that the thermal stability decreases with decreasing particle size. The ultrafine particle has significant small-size and surface effects which make it possess larger surface-area-to-volume ratio and surface bonding energy, faster mass and heat transfer, and more effective reactive collisions. Thus, through the particle refinement, the activation energy barrier is reduced and the reaction activity is elevated.

(3) In the case of the same particle size, the thermal stability is ranked in an increasing order of $Cs_2$TNR < $Rb_2$TNR < $K_2$TNR. The central metal of small atomic number has strong coordination bonding energy and therefore high stability.

(4) The 5s explosion temperature and flame sensitivity indicate that the thermal sensitivity increases as the particle size decreases, which is in good agreement with the results of thermal decomposition behavior. It suggests that the initiating mechanism of thermal decomposition is probably the same as that of thermal explosion.

(5) The particle refinement is of great significance for $M_2$TNRs to acquire the equilibrium between thermal stability and sensitivity so as to achieve the best performance and safety.

## Acknowledgement

This work was financially supported by the Science and Technology Fund on Applied Physical Chemistry Laboratory (Nos. 9140C3703051105 and 9140C370303120C37142), and the Key Support Foundation of State Key Laboratory of Explosion Science and Technology (Nos. QNKT12-02 and YBKT 10-05).

## Notes and references

1. Y. Zhang, X. Cui, F. Shi and Y. Deng, *Chemical Reviews*, 2012, **112**, 2467-2505.
2. G. Yan and M. Yang, *Organic & Biomolecular Chemistry*, 2013, **11**, 2554-2566.
3. S. Syed, A. Zubair and M. Frieri, *Current Allergy and Asthma Reports*, 2013, **13**, 50-57.
4. J. A. Hubbell and A. Chilkoti, *Science*, 2012, **337**, 303-305.
5. M. Yang, J. Yao and Y. Duan, *Analyst*, 2013, **138**, 72-86.
6. B. D. Briggs and M. R. Knecht, *Journal of Physical Chemistry Letters*, 2012, **3**, 405-418.
7. D. E. Aston, J. R. Bow and D. N. Gangadean, *International Materials Reviews*, 2013, **58**, 167-202.
8. E. Masoero, E. Del Gado, R. J.-M. Pellenq, S. Yip and F.J. Ulm, *Soft Matter*, 2014, **10**, 491-499.
9. Y. Ding and Y. Wang, *Applied Physics Letters*, 2014, **104**, 083111.
10. A. Arunkumar, D. Vanidha, K. Oudayakumar, S. Rajagopan and R. Kannan, *Journal of Applied Physics*, 2013, **114**, 183905.
11. F. Willot, L. Gillibert and D. Jeulin, *International Journal of Solids and Structures*, 2013, **50**, 1699-1709.
12. R. Liu, W. Yu, T. Zhang, L. Yang and Z. Zhou, *Physical Chemistry Chemical Physics*, 2013, **15**, 7889-7895.
13. M. Fathollahi, B. Mohammadi and J. Mohammadi, *Fuel*, 2013, **104**, 95-100.
14. H. Akkbarzade, G. A. Parsafar and Y. Bayat, *Applied Surface Science*, 2012, **258**, 2226-2230.
15. H. W. Huang, Z. B. Wang, X. P. Yong and K. Lu, *Materials Science and Technology*, 2013, **29**, 1200-1205.
16. A. K. Zak, A. M. Golsheikh, W. H. Abd Majid and S. M. Banihashemian, *Materials Letters*, 2013, **109**, 309-312.
17. A. R. Gonzalez, Y. J. O. Asencios, E. M. Assaf and J. M. Assaf, *Applied Surface Science*, 2013, **280**, 876-887.
18. S. Liu, M. Ye, A. Han and X. Chen, *Applied Surface Science*, 2014, **288**, 349-355.
19. A. Aravamudhan, D. M. Ramos, J. Nip, M. D. Harmon, R. James, M. Deng, C. T. Laurencin, X. Yu and S. G. Kumbar, *Journal of biomedical nanotechnology*, 2013, **9**, 719-731.
20. L. C. Diaz-Chacon, J. E. Arevalo-Fester, E. V. Plaza-Pirela and R. Atencio-Fuenmayor, *Acta Microscopica*, 2011, **20**, 54-59.
21. M. Pons, R. Boichot, N. Coudurier, A. Claudel, E. Blanquet, S. Lay, F. Mercier and D. Pique, *Surface & Coatings Technology*, 2013, **230**, 111-118.
22. P. Pulišová, J. Kováč, A. Voigt and P. Raschman, *Journal of Magnetism and Magnetic Materials*, 2013, **341**, 93-99.
23. G. Bahmanrokh, M. Hashim, N. Soltani, I. Ismail, P. Vaziri, M. Navaseri, M. Erfani and S. Kanagesan, *Materials Research Bulletin*, 2013, **48**, 4039-4047.
24. Y. Bayat, M. Zarandi, M. Zarei and R. Soleyman, *Journal of Molecular Liquids*, 2014, **193**, 83-86.
25. X. Mou, Y. Li, B. Zhang, L. Yao, X. Wei, D. S. Su and W. Shen, *European Journal of Inorganic Chemistry*, 2012,**16**, 2684-2690.
26. P. Alexandridis, *Chemical Engineering & Technology*, 2011, **34**, 15-28.
27. G. Liu, J. Qu and H. Wang, *Journal of Alloys and Compounds*, 2013, **578**, 345-348.
28. A. Finch and J. Payne, *Thermochimica acta*, 1990, **170**, 209-212.
29. J.W. Liu, J.G. Zhang, T.L. Zhang, D.D. Zhang and L. Yang, *Chinese Journal of Energetic Materials*, 2009, **5**, 026.
30. J. Payne, *Thermochimica acta*, 1994, **242**, 1-6.
31. J.G. Zhang, K. Wang, Z.M. Li, H. Zheng, T.L. Zhang and L. Yang, *Main Group Chemistry*, 2011, **10**, 205-213.
32. J. Payne, *Thermochimica acta*, 1994, **242**, 13-21.
33. K. Raha and J. Chhabra, *Defence Science Journal*, 2013, **41**, 21-25.
34. M. S. Refat, H. A. Saad, M. Y. El-Sayed, A. M. A. Adam, O. Z. Yeşilel and M. Taş, *Journal of Chemistry*, 2013, **2013**.
35. Z.M. Li, M.R. Zhou, T.L. Zhang, J.G. Zhang, L. Yang and Z.N. Zhou, *Journal of Materials Chemistry A*, 2013, **1**, 12710-12714.
36. J. Ledgard, *A Soldiers Handbook, Volume 1: Explosives Operations*, Department of the Army, USA, 2007.
37. L. E. Fried, M. R. Manaa, P. F. Pagoria and R. L. Simpson, *Annual Review of Materials Research*, 2001, **31**, 291-321.

38. N. Orbovic and C. L. Codoceo, *Propellants, Explosives, Pyrotechnics*, 2008, **33**, 459-466.
39. R. Liu, T. Zhang, L. Yang, Z. Zhou and X. Hu, *Central European Journal of Chemistry*, 2013, **11**, 774-781.
40. R. Liu, Z. Zhou, Y. Yin, L. Yang and T. Zhang, *Thermochimica Acta*, 2012, **537**, 13-19.
41. R. Jiang, Z. Liu, *Initiating explosive*, Ordanance Industry Press, Beijing, 2006, pp. 32-34.
42. Y. Zhao, J. Zhao, Z. Su, X. Hao, D. Ma, Y. Lu and J. Guo, *Colloids and Surfaces A: Physicochemical and Engineering Aspects*, 2013, **436**, 34-40.
43. Y. Dai and Y. Song, *Chemical Physics Letters*, 2014, **591**, 126-129.
44. C. Jo, J. Jung, H. S. Shin, J. Kim and R. Ryoo, *Angewandte Chemie*, 2013, **125**, 10198-10201.
45. J. Zhang, C. Hou, H. Huang, L. Zhang, Z. Jiang, G. Chen, Y. Jia, Q. Kuang, Z. Xie and L. Zheng, *Small*, 2013, **9**, 538-544.
46. R. Liu, S. Qi, T. Zhang, Z. Zhou, L. Yang and J. Zhang, *Chinese Science Bulletin*, 2013, **58**, 1892-1896.
47. J. Lv, L. Chen, W. Chen, H. Gao and M. Peng, *Thermochimica Acta*, 2013, **571**, 60-63.
48. L. Xue, F. Q. Zhao, R. Z. Hu and H. X. Gao, *Journal of Energetic Materials*, 2010, **28**, 17-34.
49. M. Fathollahi, B. Mohammadi and J. Mohammadi, *Fuel*, 2013, **104**, 95-100.
50. K.Z. Xu, X.G. Zuo, H. Zhang, B. Yan, J. Huang, H.X. Ma, B.Z. Wang and F.Q. Zhao, *Journal of Thermal Analysis and Calorimetry*, 2012, **110**, 585-591.
51. R. Z. Hu, S. L. Gao, F. Q. Zhao, Q. Z. Shi, T. L. Zhang and J. J. Zhang, Thermal Analysis Kinetics second ed, Science Press, Beijing, 2008.
52. Q.L. Yan, M. Künzel, S. Zeman, R. Svoboda and M. Bartošková, *Thermochimica Acta*, 2013, **566**, 137-148.
53. M. Che and J. C. Védrine, *Characterization of solid materials and heterogeneous catalysts: From structure to surface reactivity*, John Wiley & Sons, 2013.
54. C. Fischer, I. Kurganskaya, T. Schäfer and A. Lüttge, *Applied Geochemistry*, 2014, **43**, 132-157.
55. S. Selcµk and A. Selloni, *The Journal of Physical Chemistry C*, 2013, **117**, 6358-6362.
56. H. Wang, G. Jian, S. Yan, J. B. DeLisio, C. Huang and M. R. Zachariah, *ACS applied materials & interfaces*, 2013, **5**, 6797-6801.
57. A. K. Galwey, D. G. Bettany and M. Mortimer, *International Journal of Chemical Kinetics*, 2006, **38**, 689-702.
58. J. G. R. Poco, H. Furlan and R. Giudici, *Journal of Physical Chemistry B*, 2002, **106**, 4873-4877.
59. S. Vyazovkin, A. K. Burnham, J. M. Criado, L. A. Perez-Maqueda, C. Popescu and N. Sbirrazzuoli, *Thermochimica Acta*, 2011, **520**, 1-19.
60. Q.L. Yan, S. Zeman, J. Šelešovský, R. Svoboda and A. Elbeih, *Journal of Thermal Analysis and Calorimetry*, 2013, **111**, 1419-1430.
61. B. V. L'vov and A. K. Galwey, *International Reviews in Physical Chemistry*, 2013, **32**, 515-557.
62. D. L. Reid, K. R. Kreitz, M. A. Stephens, J. E. S. King, P. Nachimuthu, E. L. Petersen and S. Seal, *Journal of Physical Chemistry C*, 2011, **115**, 10412-10418.
63. M. Fathollahi, S. M. Pourmortazavi and S. G. Hosseini, *Journal of Energetic Materials*, 2008, **26**, 52-69.
64. GJB 772A-97, Method 501.2: *Vacuum stability test - Method of pressure transducer*, Commission of Science, Technology and Industry for National Defense, Beijing, 1997, pp. 156-158.
65. GJB 5891.12-2006, *Test method of loading material for initiating explosive device - Part 12: Vacuum stability test - Method of pressure transducer*, Commission of Science, Technology and Industry for National Defense, Beijing, 2006, pp. 67-70.
66. GJB 5891.20-2006, *Test method of loading material for initiating explosive device. Part 20: Measurement of deflagration point for primary explosive - Method of 5s delay time*, Commission of Science, Technology and Industry for National Defense, Beijing, 2006, pp. 119-122.
67. GJB 5891.25-2006, *Test method of loading material for initiating explosive device. Part 25: Sensitivity to flame test*,

Commission of Science, Technology and Industry for National Defense, Beijing, 2006, pp. 149-153.

68. M. A. Wood, A. C. van Duin and A. Strachan, *The Journal of Physical Chemistry A*, 2014, **5**, 885-895.

69. M. Künzel, Q.L. Yan, J. Šelešovský, S. Zeman and R. Matyáš, *Journal of Thermal Analysis and Calorimetry*, 2014, **115**, 289-299.

70. O. Sharia, R. Tsyshevsky and M. M. Kuklja, *The Journal of Physical Chemistry Letters*, 2013, **4**, 730-734.